

## Raman spectra and athermal laser annealing of $\text{Ge}(\text{S}_x\text{Se}_{1-x})_2$ glasses

J. E. Griffiths, G. P. Espinosa, J. C. Phillips, and J. P. Remeika

*Bell Laboratories, Murray Hill, New Jersey 07974*

(Received 24 January 1983)

We have measured and interpreted the Raman spectra of bulk  $\text{Ge}(\text{S}_x\text{Se}_{1-x})_2$  glasses for compositions in the range  $0 \leq x \leq 0.25$ , both at low power levels and at sufficiently high power levels to induce thermally reversible (at  $T \lesssim T_g/2$ ) athermal microcrystallization. Substitution of Se by S in  $\text{Ge}(\text{Se}_{1/2})_4$  tetrahedra produced narrow satellites to the narrow  $A_1$  symmetric breathing mode which are easily resolved. The splittings of these satellites are compared to those of the corresponding molecular lines of  $\text{GeCl}_n\text{Br}_{4-n}$  and are the basis for the molecular models discussed in the accompanying paper of Aronovitz *et al.* Athermal microcrystallization is achieved near liquid-nitrogen temperature. Addition of S up to  $x = 0.25$  is found to inhibit but not prevent thermal revitrification at room temperature  $T_r \sim T_g/2$  on a time scale of hours.

### I. INTRODUCTION

Two models of atomically disordered solids have been widely discussed in the scientific and technological literature, based on clusters or on "randomness." Diffraction data have yielded relatively little direct information about the structure on an atomic scale of disordered solids. The limitations of this direct approach have led many Western scientists to adopt "random" models of the atomic structure of disordered solids, e.g., random-network models of insulating glasses and random-packing models of metallic glasses.<sup>1-6</sup>

The most appealing aspect of these models is their simplicity. However, if we restrict our attention to the network materials (such as  $\text{SiO}_2$  and  $\text{As}_2\text{S}_3$ ) which are very good glass formers, the random models appear to be insufficient to explain the origin of the glass-forming tendency. At normal cooling rates of order 10 K/min these materials do not crystallize and their viscosities in the supercooled melt may become as large as  $10^{13}$  P or more. It is natural to associate these gigantic viscosities with the formation of large molecular clusters such as are responsible for the large viscosities of excellent organic glass formers such as glycerine or glucose. These clusters may be analogous to the "vitroids" discussed in the literature.<sup>7-9</sup>

The next step in understanding the structure of inorganic glasses lies in the construction of specific molecular models for the glass-forming clusters. The most obvious choice for the cluster structure is that of the high-temperature crystalline phase, the first phase nucleated from the liquid. The problem raised by this choice is that one must then be able to reconstruct the cluster surface in such a way that the reconstruction is metastable, costs little enthalpy, and at the same time presents a barrier to crystallization.

Recently great attention has focused on the materials  $\text{GeS}_2$  and  $\text{GeSe}_2$  because it has become apparent that Raman spectroscopy is a simple, direct, and powerful probe

of the molecular structure of chalcogenide glass alloys,<sup>10-17</sup> and that the spectra of these compounds are particularly easy to interpret. By extending this work we were able to show<sup>18</sup> that all the available data do indeed point to the presence of large partially polymerized clusters in  $g\text{-GeS}_2$  and  $g\text{-GeSe}_2$ , and that many of these large clusters are fragments of the high-temperature layer structures which are terminated on their lateral edges by chalcogen dimers. At the stoichiometric composition, the chalcogen edge dimer bonds are compensated by Ge-Ge bonds in ethanelike polymerized clusters<sup>14,15</sup> whose vibrations are recognizable in the Raman spectra. Many of the structural details of this model have been clarified and extended by recent Mössbauer studies.<sup>19-22</sup>

Having established the nature of the static structure of  $\text{GeS}_2$  and  $\text{GeSe}_2$  glasses we can now consider possible dynamic phenomena. The most interesting of these is athermal (i.e., essentially neither thermal nor nonthermal) laser annealing<sup>23</sup> which is a very striking and dramatic phenomenon which should not be confused with conventional laser annealing by heating. (Heating, of course, takes place, but it is incidental rather than essential.) Hajtő and co-workers were the first to discover evidence indicative of athermal behavior in optical switching of  $\text{GeSe}_2$  films by Urbach-tail laser beams.<sup>24,25</sup> The origin of this remarkable behavior was explained by us<sup>23,26</sup> in terms of reversible microcrystallization induced by pumping of the chemical disorder (like-atom bonds) which is characteristic of the structure of the partially polymerized clusters in these materials. In this process the information on bond strength carried by the Urbach-tail photons plays a crucial role. According to our model, similar effects have not been observed with  $g\text{-As}_2(\text{S,Se})_3$  samples because the chemical order cannot be pumped optically, although similar heating effects accompany photon absorption. More recently Hajtő and co-workers have discovered that Urbach-tail photons can induce optical anisotropy in  $\text{GeSe}_2$  films.<sup>27</sup> They explained this phenomenon in terms

of laser-induced orientation of the (dimerized raftlike) clusters<sup>18</sup> which in the crystal produces optical anisotropy.<sup>28</sup> In this case similar effects associated with reorientation of layerlike units have been observed in *g*-As<sub>2</sub>(S,Se)<sub>3</sub> by Malinovsky *et al.*<sup>27</sup> These reorientation effects are due to local heating and dielectric anisotropy and are in agreement with raftlike models of molecular clusters in these materials.<sup>28</sup>

In this paper we continue our dynamic studies of these glasses by studying the behavior of Ge(S<sub>x</sub>Se<sub>1-x</sub>)<sub>2</sub> alloys for 0 ≤ *x* ≤ 0.25. We have found, as expected, many similarities between the dynamical behavior of GeS<sub>2</sub> (not reported here) and GeSe<sub>2</sub>, but significant differences as well which may be related in part to the existence of two crystal structures in GeS<sub>2</sub> with a transition temperature *T<sub>c</sub>* > *T<sub>g</sub>*. Specifically, reversibility of quasicrystallization and microcrystallization<sup>26</sup> is more difficult to achieve<sup>29</sup> in GeS<sub>2</sub>.

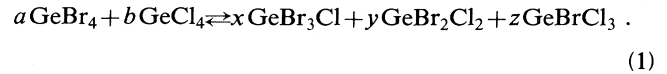
Partial substitution of Se in GeSe<sub>2</sub> with smaller and more electronegative sulfur atoms to form, for example, GeS<sub>0.25</sub>Se<sub>1.75</sub>- and GeSe<sub>0.5</sub>Se<sub>1.5</sub>-alloy glasses can lead to further complications. On average, in GeS<sub>0.5</sub>Se<sub>1.5</sub>, one might reasonably expect that the predominant tetrahedral structural units in the melt would be GeSe<sub>4</sub> and GeSSe<sub>3</sub>, analogous to the well-known GeBr<sub>3</sub>Cl molecular species. Drawing such an analogy can be extremely useful in understanding the formation of transitory products in chemical reactions occurring in the melt before quenching. It is also a useful starting point for identifying the nature of the tetrahedral building blocks in the quenched glass in much the same way as was done earlier by comparing the observed vibrational spectra of molecular GeCl<sub>4</sub> and GeBr<sub>4</sub> with *g*-GeS<sub>2</sub> and *g*-GeSe<sub>2</sub>, respectively.<sup>13,18</sup>

The microscopic structures of the GeS<sub>x</sub>Se<sub>2-x</sub> (0.06 < *x* < 0.5) alloys are not known at this time nor is anything known about the chemical constitution and structural distribution of the tetrahedral building blocks and *wrong* bonds in such materials.<sup>30</sup> One might expect Se—Se, Se—S, and S—S bond types to be present with the Se-Se cluster-size-limiting dimer bonds predominating at these selenium-rich glass compositions. Arguments based on relative bond energies, bond angles, and bond distances would favor the sulfur atoms being incorporated within the body of the clusters. To minimize strain, the sulfur atoms are more likely to assume positions linking tetrahedra at corners rather than at edges. Under such conditions, we may expect that photon-induced microcrystallization may most probably be initiated at the cluster edges under laser-flux conditions comparable to that observed for pure GeSe<sub>2</sub> glass itself.

In the present study of the GeS<sub>x</sub>Se<sub>2-x</sub> (*x* = 0.063, 0.125, 0.25, and 0.50) glass alloys we shall consider first the probable chemical reactions in the melt and the chemical constitution of the system following rapid quenching (Sec. II). The effect of photon irradiation of the glasses will be discussed in Sec. III. Experimental details appear in Sec. IV. A microscopic theoretical model and experimental results are presented in Sec. V. A summary of the overall picture which has emerged concerning structure and phototransformation kinetics is given in Sec. VI.

## II. CHEMICAL REACTIONS IN THE Ge-S-Se SYSTEM

The thermally activated reactions of gaseous and liquid GeBr<sub>4</sub> with GeCl<sub>4</sub> leading to a redistribution of Ge—Br and Ge—Cl bonds have been studied extensively.<sup>31-33</sup> The appropriate generalized equilibrium can be expressed as



By appropriate selection of the *a/b* ratio, the product distribution may be directed to favor any of the individual tetrahedral mixed-halide compounds but not to the exclusion of the others. In pure GeSe<sub>2</sub> and GeS<sub>2</sub> the basic tetrahedral structural units are (GeSe<sub>4</sub>) and (GeS<sub>4</sub>) which are bridged to each other to preserve valence and coordination requirements. Each germanium atom is bonded to four chalcogenide atoms and each chalcogenide to two germaniums. For elevated temperatures, the behavior of a melt containing germanium, sulfur, and selenium is expected to be similar to a mixture of GeBr<sub>4</sub> and GeCl<sub>4</sub>. Thus, for a composition corresponding to GeS<sub>0.5</sub>Se<sub>1.5</sub> (GeBr<sub>3</sub>Cl), one might anticipate the following processes to occur in the melt:



where intraspecies bonding would be an important aspect of the resulting structures. Such bonding would preserve to a large extent the chemical constitution of the tetrahedra present in the liquid and gas phases. Thus, upon quenching, the glass may be expected to consist of linked tetrahedra of (GeSe<sub>4</sub>), (GeSe<sub>3</sub>S), (GeSe<sub>2</sub>S<sub>2</sub>), (GeSeS<sub>3</sub>), and (GeS<sub>4</sub>) in diminishing proportions analogous to molecular GeBr<sub>4</sub>, GeBr<sub>3</sub>Cl, GeBr<sub>2</sub>Cl<sub>2</sub>, GeBrCl<sub>3</sub>, and GeCl<sub>4</sub> that would result from heating a mixture of GeBr<sub>4</sub> and GeCl<sub>4</sub>. The initial composition, being selenium rich, would favor (GeSe<sub>4</sub>)-, (GeSe<sub>3</sub>S)-, and (GeSe<sub>2</sub>S<sub>2</sub>)-linked tetrahedra in decreasing order. Evidence for such reactions and tetrahedral species is expected to be found in the Raman spectra of the quenched glass.

The various tetrahedra proposed above are expected to link and crosslink in much the same manner as in pure GeSe<sub>2</sub> and GeS<sub>2</sub> resulting in a system of weakly coupled oscillators whose Raman spectrum will be dominated by the relatively narrow symmetric stretching mode *ν*<sub>1</sub> for each kind of tetrahedron. All of the other Raman-active modes will be observable, but because each is expected to be much less intense, broader, and less well defined than *ν*<sub>1</sub>, they will be extensively overlapped with each other and hence less useful as identification tools for specific tetrahedra. It is already well established that the frequency ratios *ν*<sub>1</sub>(GeBr<sub>4</sub>)/*ν*<sub>1</sub>(GeSe<sub>2</sub>) = *ν*<sub>1</sub>(GeCl<sub>4</sub>)/*ν*<sub>1</sub>(GeS<sub>2</sub>) are equal to within about 0.25%. Therefore, one may anticipate that similar frequency scaling should occur for the mixed halides and mixed chalcogenides. It will be shown in Sec. V that this is true and is useful in delineating some features of the complex Raman spectra of the glasses under study here.

As in the case of  $\text{GeSe}_2$ , rapid quenching of the melt is expected to freeze in the composition of the tetrahedra. Because chemical reorganization is inhibited by the time scale of the quenching, some wrong bonds are expected to form of which Se—Se, Se—S, S—S, and Ge—Ge are representative. The number of broken coordination constraints (departures from the  $8-N$  rule or simply broken bonds) is assumed negligible.

Given that such bonds occur as they do in  $\text{GeSe}_2$  glass, it is another matter to detect them in the spectra of the mixed-chalcogenide alloys. Both mass and force-constant considerations suggest that Raman bands due to chalcogenide wrong bonds will occur in the same spectral range as the  $\nu_1$  modes of the mixed-chalcogenide tetrahedra and may be completely masked. The Ge—Ge wrong-bond vibrational modes may be identifiable, however, because they will occur on the low-frequency side of the  $\nu_1$ -band profile of the linked  $\text{GeSe}_4$  species. Moreover, the Ge—Ge bond-stretch symmetry coordinate involves mainly an oscillating motion of the  $\text{GeS}_n\text{Se}_{3-n}$  ( $n=0-3$ ) units away from and toward each other so that the masses of the chalcogenides will have a much smaller effect upon the frequency than on those modes involving motions mainly of the chalcogenide atoms themselves. Thus the frequency of the Ge—Ge wrong-bond stretching motion will not be affected as strongly by the sulfur substitution.

Lowering the sulfur content to  $\text{GeS}_{0.25}\text{Se}_{1.75}$  is equivalent to changing the  $a/b$  mole ratio in Eq. (1) from 4 in  $\text{GeS}_{0.5}\text{Se}_{1.5}$  to 7. The effect on the overall vibrational spectra will not be so much on the observed frequencies of the bands arising from motions within specific linked tetrahedra as on the relative strengths of the same bands. This will also be true when  $x$  is reduced further to 0.125 and 0.063.

### III. EFFECT OF PHOTON IRRADIATION

Quenching the well-mixed high-temperature system initially containing elemental germanium, sulfur, and selenium, and subsequent mixing of complex chemical species capable of extensive bond linking and crosslinking, is expected to produce considerable anion disorder as discussed in Sec. II. The mixed-chalcogenide alloys are strongly absorbing with band edges closer to that of  $\text{GeSe}_2$  than to  $\text{GeS}_2$ , reflecting the selenium-rich initial composition. Therefore, like  $\text{GeSe}_2$ , absorption of photons with energies outside the absorption edge in the Urbach tail can break wrong bonds preferentially, thereby allowing more ordering to occur at the short- and intermediate-range level. This is expected to reduce the initial randomness present in the as-prepared glass by allowing highly strained mixed-chalcogenide tetrahedra to rearrange into polymeric clusters with substantial intermediate-range order. The resulting material, however, will still maintain the macroscopic properties of a glass containing loosely coupled tetrahedral structural units such as  $(\text{GeSe}_3\text{S})$ ,  $(\text{GeSe}_2\text{S}_2)$ , and  $(\text{GeSeS}_3)$ . Such tetrahedra, when they form in the melt or link and crosslink as a result of photon-induced reorganization in the glass phase, should be identifiable from their Raman spectra. The symmetric stretching vibrations for each species will dominate by virtue of their

expected strong intensities, narrow-band contours, and mass-dependent frequencies. Thus, the order of frequencies for the individual  $\nu_1$ -type modes is expected to be  $(\text{GeSe}_4) < (\text{GeSe}_3\text{S}) < (\text{GeSe}_2\text{S}_2) < (\text{GeSeS}_3) < (\text{GeS}_4)$  based on data already available for the germanium bromochlorides.<sup>33</sup>

When the laser power is increased further, more extensive structural reorganization is expected, much as in the case of  $\text{GeSe}_2$ ,<sup>18,26</sup> ultimately leading to microcrystallization. Whether the initial intracluster reorganization of tetrahedra, which increases intermediate- and short-range order, or the microcrystallization process, which involves an increase in long-range order, will be reversible or not, cannot be predicted with confidence for the mixed-chalcogenide system. It will be shown in later sections, however, that the initial photon-induced structural reorganization is not reversible largely because it involves processes mainly occurring at short range and that the photon-induced long-range ordering to form microcrystallites is indeed reversible, albeit with more difficulty than for pure  $\text{GeSe}_2$ , upon removal of the photon flux. The latter depends in part on the fraction of the irradiated volume that has been converted to microcrystallites.

## IV. EXPERIMENTAL

### A. Preparation and characterization of glasses

In a typical synthesis, powdered germanium (99.999% purity), previously vacuum-melted selenium (99.999% purity), and sulfur (99.999% purity) were weighed ( $\pm 0.0001$  g) in appropriate mole ratios and sealed under vacuum in a 6-cm fused-silica tube (6 mm i.d.). Mixtures of compositions  $\text{GeS}_{0.25}\text{Se}_{1.75}$  and  $\text{GeS}_{0.5}\text{Se}_{1.5}$  were heated at 1025 and 905 °C, respectively, for 3 h with intermittent rocking of the sample tubes to ensure mixing before quenching directly from the furnace into water. The heating temperature for  $\text{GeS}_{0.063}\text{Se}_{1.937}$  and  $\text{GeS}_{0.125}\text{Se}_{1.875}$  was 905 °C but the former was held at that temperature for 16 h before quenching. Clear red glasses resulted in all cases.

Samples ( $70 \pm 0.1$  mg) were characterized by their differential thermal-analysis patterns using a model-990 DuPont thermal-analysis instrument fitted with a high-temperature (1600 °C) differential-thermal-analysis (DTA) cell. This was heated at a constant rate of 10 °C/min under argon. Data for two samples are shown in Fig. 1 and are listed for all samples in Table I.

### B. Raman experiments

Irregularly shaped samples were available from the silica preparation tubes. A piece was mounted on the copper cold finger of an evacuated ( $10^{-5}$  Torr) liquid-nitrogen-cooled Air Products cryostat via thermal grease (Air Products) in such a way that the very smooth external curved surface shaped by the original sample tube was presented to the incoming laser beam. The beam at 647 nm from a Spectra-Physics 164 krypton-ion laser entered

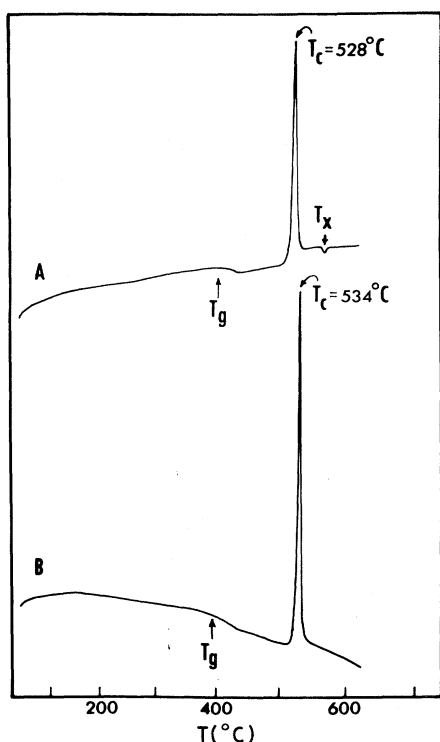


FIG. 1. DTA patterns for (a)  $\text{GeS}_{0.5}\text{Se}_{1.5}$  and (b)  $\text{GeS}_{0.25}\text{Se}_{1.75}$  glass alloys. Glass transition temperatures  $T_g$  and crystallization temperatures  $T_c$  are marked.

the sample at about  $70^\circ$  to the surface normal and scattered light was collected at  $90^\circ$  to the incident beam. The electric vector of the laser beam was either in the plane of incidence ( $H$  polarization) or perpendicular ( $V$  polarization) to it. Most experiments utilized  $H$  polarization so that penetration of the beam was favored over reflection.

Scattered light was analyzed using an Instruments S. A. Ramanor HG-2S spectrophotometer equipped with photon-counting electronics. A Data-General Eclipse S-130 minicomputer was used to control the experiments and collect data. Except where noted all data were digital and sample temperatures were nominally  $-196^\circ\text{C}$ .

TABLE I. DTA data for  $\text{GeS}_x\text{Se}_{2-x}$  glasses.

Sample stoichiometry	$T_c^a$ ( $^\circ\text{C}$ )	$T_g^b$ ( $^\circ\text{C}$ )	$T_m^c$ ( $^\circ\text{C}$ )
$\text{GeSe}_{2.0}$	533	392	740
$\text{GeS}_{0.50}\text{Se}_{1.50}$	528	402	
$\text{GeS}_{0.25}\text{Se}_{1.75}$	534	394	
$\text{GeS}_{0.125}\text{Se}_{1.875}$	521	396	
$\text{GeS}_{0.063}\text{Se}_{1.937}$	518	390	
$\text{GeS}_{2.0}$	511	463	850

<sup>a</sup>Crystallization temperature.

<sup>b</sup>Glass transition temperature; note that the transition is broad and weak (Fig. 1).

<sup>c</sup>Melting point.

## V. RESULTS

### A. DTA results

The glass transition temperature  $T_g$  and the crystallization temperature for stoichiometric  $\text{GeSe}_2$  glass are  $T_g \approx 392^\circ\text{C}$  and  $T_c = 533^\circ\text{C}$ , respectively.<sup>34</sup> These may be compared with the crystalline melting point  $T_m = 740^\circ\text{C}$ . Corresponding values for  $\text{GeS}_2$  are listed in Table I.  $T_c$  is strongly dependent on the  $[\text{Se}]/[\text{Ge}]$  ratio.<sup>3</sup> When the glass is only slightly germanium rich, a weak high-temperature endotherm occurs at  $570 \leq T_x \leq 575^\circ\text{C}$  in the DTA pattern. The presence of this endotherm appears to arise from a solid solubility of minute amounts of  $\text{GeSe}$  in  $\text{GeSe}_2$  and may cause a drop in  $T_c$ .<sup>3</sup>

In the present work, materials had the nominal compositions  $\text{GeS}_x\text{Se}_{2-x}$  ( $x \approx 0.063, 0.125, 0.25,$  and  $0.5$ ) having  $T_c$  values of 518, 521, 534 and  $528^\circ\text{C}$ , respectively (see Fig. 1 and Table I). The  $\text{GeS}_{0.5}\text{Se}_{1.5}$  sample also showed a small endotherm at  $T_x = 570^\circ\text{C}$  of the type discussed above. The presence or absence of such an endotherm, provided it is small, will have a negligible effect on the Raman scattering results.<sup>3</sup> The sharpness of the  $T_c$  exotherms indicates the absence of compound separation ( $\text{GeSe}_2$  and  $\text{GeS}_2$ ) on crystallization and that the chalcogenide to germanium ratio is very close to 2. Thus, the samples are homogeneous glasses and not intimate microscopic mixtures of  $\text{GeSe}_2$  and  $\text{GeS}_2$ .

### B. Raman spectra

To aid in understanding the behavior of the mixed-chalcogenide glass alloys of germanium under photon irradiation, it is useful to correlate the observed Raman spectra of the various mixed molecular halides  $\text{GeBr}_x\text{Cl}_{4-x}$ , which are well understood, with those of the pure  $\text{GeSe}_2$  and  $\text{GeS}_2$  glasses in terms of symmetry coordinates. This is possible in a qualitative way because of the relatively weak coupling between linked  $(\text{GeSe}_4)$  and  $(\text{GeS}_4)$  tetrahedra in the glasses. A detailed correlation diagram is shown in Fig. 2 in which the various vibrational energy levels for all the fundamental modes of the  $\text{GeBr}_x\text{Cl}_{4-x}$  ( $x = 0-4$ ) molecular species appear as solid horizontal lines. Spectra of the pure  $\text{GeSe}_2$  and  $\text{GeS}_2$  glasses appear along the left- and right-hand margins, respectively. (The low-frequency "Böse" peaks near  $20\text{ cm}^{-1}$  are not shown.) In the weak coupling limit, the totally symmetric breathing modes of the  $(\text{GeSe}_4)$  and  $(\text{GeS}_4)$  units are easily identified by their relatively narrow-band contours, large scattering strengths, and low depolarization ratios. These glass modes correspond to the  $\nu_1(a_1)$  modes found in molecular  $\text{GeBr}_4$  and  $\text{GeCl}_4$ , respectively. Solid arrows in Fig. 2 show this correlation which has been discussed earlier by Kumagai *et al.*<sup>18</sup> For the degenerate modes, corresponding to the  $\nu_2(e)$ ,  $\nu_3(f_2)$ , and  $\nu_4(f_2)$  normal modes in the molecular tetrahalides, the correlation is less convincing because the weak coupling limit begins to break down. The appropriate bands in the glasses are in general much broader. Those corresponding to  $\nu_3$  appear at a lower frequency while those corresponding in a rough way with  $\nu_2$  and  $\nu_4$  appear at

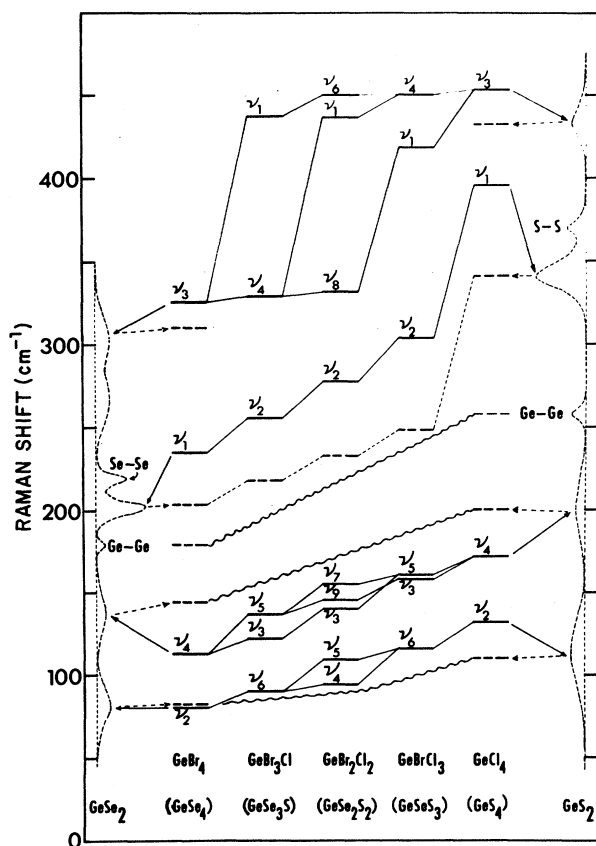


FIG. 2. Correlation diagram for mixed molecular chlorobromogermanes and  $\text{GeS}_x\text{Se}_{2-x}$  glass alloys. Solid line denotes vibrational energy levels for the chlorobromogermanes listed at the bottom. Dashed line denotes energy levels for the  $(\text{GeS}_x\text{Se}_{4-x})$  components of the glass alloys. Representative spectra of pure  $\text{GeSe}_2$  and  $\text{GeS}_2$  glasses without their Böse peaks are along the left-hand and right-hand margins, respectively. Solid arrows at the left and right show the approximate correlations of vibrational modes between  $\text{GeSe}_2$  and  $\text{GeBr}_4$  and between  $\text{GeS}_2$  and  $\text{GeCl}_4$ . Dashed arrows reconnect the spectral bands of  $\text{GeSe}_2$  and  $\text{GeS}_2$  with the observed bands in the  $\text{GeS}_x\text{Se}_{2-x}$  glass alloys (left-hand side) and for convenience with pure  $\text{GeS}_2$  (right-hand side). Wrong-bond Ge—Ge, Se—Se, and S—S bands are labeled. Wavy lines connect energy levels at the left-hand and right-hand sides for cases where no specific assignments are practical. Mode numbering follows the Herzberg convention. Note specifically that in the mixed-anion case,  $\nu_2$  corresponds to  $\nu_1$  of pure anions, etc.

equal or higher frequencies. These correlations are also shown by solid arrows. Because of the reduced scattering strengths and extreme breadths of the modes corresponding to  $\nu_2$ ,  $\nu_3$ , and  $\nu_4$ , as contrasted with the narrow-band contours and strong intensities of the  $A_1$  modes, the spectra of the latter are likely to be much more informative in glass alloys containing both sulfur and selenium and concomitantly the mixed  $(\text{GeS}_x\text{Se}_{4-x})$  linked tetrahedra. Extending the empirical frequency scaling relationships<sup>18</sup> for the so-called  $\nu_1$  mode where

$$\frac{\nu_1(\text{GeBr}_4)}{\nu_1(\text{GeSe}_2)} = \frac{\nu_1(\text{GeCl}_4)}{\nu_1(\text{GeS}_2)} = 1.16$$

to the mixed chlorobromides and sulfur selenides, one may predict the energy values of the corresponding  $\nu_1$ -type modes to be at 222.4 ( $\text{GeSe}_3\text{S}$ ), 243.1 ( $\text{GeSe}_2\text{S}_2$ ), and 266 ( $\text{GeBrCl}_3$ )  $\text{cm}^{-1}$  (Table II). The measured values, which are shown (dashed levels) in Fig. 2 and Table II and will be discussed below, are in reasonable agreement with predictions. As the  $[\text{S}]/[\text{Se}]$  composition ratio in the tetrahedra increases, agreement becomes progressively worse. This would suggest increasing intratetrahedral coupling in the more sulfur-rich tetrahedral units. Broken arrows show the correlations in Fig. 2. The other bands, because of their breadth, are less informative; wavy connecting lines join the extremes for  $\nu_2$  and  $\nu_4$ . The  $\nu_3$  modes are left unconnected for clarity.

The bands due to wrong bonds, Ge—Ge, Se—Se, and S—S, which have no counterparts in the spectra of the molecular chlorobromides, are also identified in Fig. 2. The Ge—Ge band is connected with a wavy line but the Se—Se and S—S pairs are not connected. It is not practical to discuss these modes in detail because it is obvious that their identification in pseudobinary spectra is highly unlikely. The Se—Se, S—Se, and S—S ones will be masked by the  $\nu_1$ -like modes of the  $(\text{GeS}_x\text{Se}_{4-x})$  tetrahedra and the  $\nu_3$ -like modes of all species. For low-sulfur-content materials of the kind under study here, the Ge—Ge wrong-bond band should be readily identifiable on the low-frequency side of the main band system starting near 200  $\text{cm}^{-1}$ . The extreme breadth of the  $\nu_3$ -like mode in  $\text{GeSe}_2$  glass and its double-maximum contour has already been noted.<sup>26</sup>

Four compositions of glass alloys were studied,  $\text{GeS}_x\text{Se}_{2-x}$  ( $x = 0.063, 0.125, 0.25, \text{ and } 0.5$ ). The first two and the fourth were quenched from 905°C and the third from 1025°C. *A priori*, the most probable tetrahedral units for the last three alloys are  $\text{GeSe}_4$  and  $\text{GeSSe}_3$ . In the region near 200  $\text{cm}^{-1}$ , *A* of Fig. 3 shows for the  $x = 0.5$  alloy two relatively prominent and narrow bands at 203 and 181  $\text{cm}^{-1}$  corresponding to  $\nu_1$  of a  $(\text{GeSe}_4)$  tetrahedral unit and the Ge—Ge wrong-bond stretching mode. The balance of the spectrum consists of broad bands including several unresolved peaks between 210 and 260  $\text{cm}^{-1}$  reflecting considerable structural disorder and a low-frequency Böse peak characteristic of a glass. The spectrum, although it contains elements of similarity to that of  $\text{GeSe}_2$ , also contains several important differences. The 212- $\text{cm}^{-1}$  companion line of *g*- $\text{GeSe}_2$ , if it exists in

TABLE II. Raman frequencies ( $\text{cm}^{-1}$ ) of  $\nu_1$  modes of linked  $(\text{GeS}_x\text{Se}_{4-x})$  tetrahedra.

Species	Glass		Calculated
	$\text{GeS}_{0.5}\text{Se}_{1.5}$ Observed	$\text{GeS}_{0.25}\text{Se}_{1.75}$ Observed	
$(\text{GeSe}_4)$	204	203	202
$(\text{GeSe}_3\text{S})$	218	218	222.4
$(\text{GeSe}_2\text{S}_2)$	232	232	243.1
$(\text{GeSeS}_3)$	248	244	266

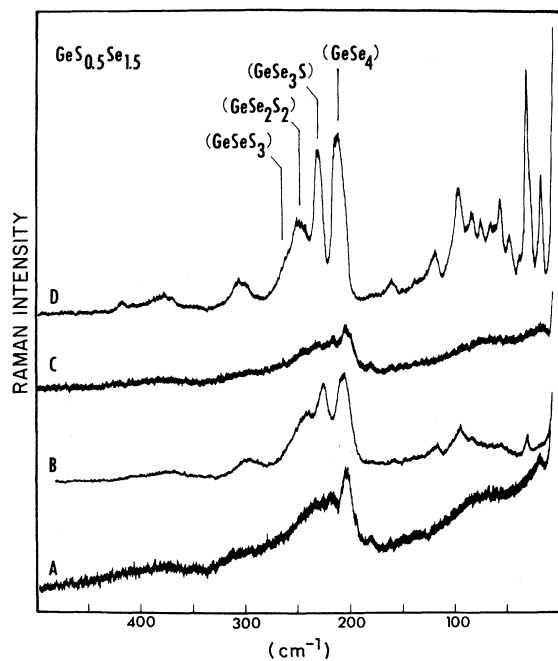


FIG. 3. Analog Raman spectra of  $\text{GeS}_{0.5}\text{Se}_{1.50}$  glass alloy. Experimental parameters: sample temperature,  $25^\circ\text{C}$ ; scan rate,  $20\text{ cm}^{-1}/\text{min}$ ; sensitivity, *A* and *C*,  $1500\text{ c/s}$  full scale, *B* and *D*,  $3000\text{ c/s}$  full scale; time constant, 1 sec; and spectral slit width,  $2.5\text{ cm}^{-1}$ . Laser power (in mW) ( $647.1\text{ nm}$ ): *A*, 11 and *B*, 69; sample allowed to relax overnight at room temperature in the dark before recording; *C*, 11 mW; power raised to 80 mW for 1 h before recording *D* at 11 mW.

$g\text{-GeS}_{0.5}\text{Se}_{1.5}$ , is masked by the several broad  $\nu_1$  Raman bands between  $210$  and  $260\text{ cm}^{-1}$ .

At a higher power level (69 mW, *B*, Fig. 3), the uncertainties in the spectra are clarified through several dramatic changes. In the very-low-frequency regime the disappearance of the Böse peak and the growth of the

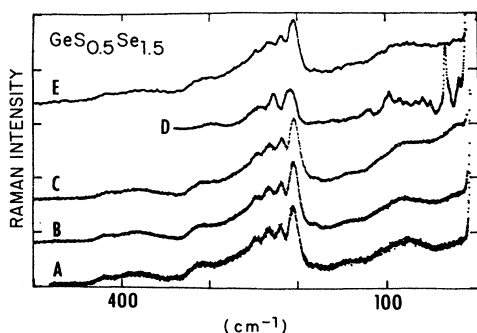


FIG. 4. Raman spectra of  $\text{GeS}_{0.5}\text{Se}_{1.5}$  glass alloy at  $-196^\circ\text{C}$ . Experimental parameters: scan step size,  $0.2\text{ cm}^{-1}$ , except *C*  $0.4\text{ cm}^{-1}$ ; count time/step (in sec), *A* 1.5, *B* 0.7, *C* 0.1 (seven scans), *D* 0.2, *E* 0.3; spectral slit width,  $3.7\text{ cm}^{-1}$ . Data smoothing: *D* 17-point Savitsky-Golov technique; *E* fast-Fourier-transform technique using a 15-ps exponential filter. Laser excitation (in mW) ( $647.1\text{ nm}$ ): *A*, 4.8; *B*, 48; *C*, 72; *D*, 122; sample allowed to relax overnight at room temperature in the dark before recording *E* 16.

crystallineline at  $31\text{ cm}^{-1}$  signals the first stage<sup>18,26</sup> of photon-induced microcrystallization. Coincident with this change in intermediate-range order is the reorganization of mixed-chalcogenide tetrahedra into more easily identifiable units. The frequencies of the strong bands at  $207$ ,  $227$ , and  $242\text{ cm}^{-1}$  are readily interpretable as the  $\nu_1$  modes of  $\text{GeSe}_4$ ,  $\text{GeSe}_3\text{S}$ , and  $\text{GeSe}_2\text{S}_2$  tetrahedra, and their frequencies agree rather well with the predicted values (see above).

Relaxation of the system in the dark at  $T < T_g/2$  leads to *C*, Fig. 3, where features due to long-range order (crystallinity) have disappeared and the system is again glass-like. Perhaps because of residual stress the  $\text{GeSe}_4$ ,  $\nu_1$ -mode-scattering strength is reduced compared to the virgin glass. Unchanged, however, is the short- and intermediate-range order due to the existence of mixed-chalcogenide tetrahedra. The definition of particular tetrahedra in terms of spectral features is reduced but vestiges of the four peaks seen in the virgin glass in Fig. 3 *A* still are observable in Fig. 3 *C* in the range  $207\text{--}245\text{ cm}^{-1}$ . In this case the band most likely due to  $\text{GeSe}_3$  at  $247\text{ cm}^{-1}$  is barely discernible.

When the laser power is increased to a higher level (80 mW) than in Fig. 3 *B* for 1 h and the spectrum recorded at low power (11 mW), extensive long-range order is revealed through many low-frequency lattice bands, which signal the formation of microcrystallites [Fig. 3 *D*]. Comparison of this spectrum with Fig. 3 *B* shows enormous changes especially at low frequencies. The  $31\text{-cm}^{-1}$  band is now the most intense. The  $\nu_1$  region is also well defined, although the full width at half-maximum of each band is at least  $15\text{ cm}^{-1}$ . In crystalline  $\text{GeSe}_2$ , the bandwidth is  $3.0\text{ cm}^{-1}$ . Notably absent in Figs. 3 *B* and 3 *D* is evidence of the bands due to either Se-Se or Ge-Ge chemically disordered ("wrong") bonds. This disappearance is expected for systems of this kind where long-range ordering driven by photoinduced chemical ordering begins to dominate the structure. Ordering to a crystalline phase is not complete, however. Linewidths are too broad, and therefore microcrystallites in a glass matrix is a more reasonable interpretation.

Figures 4–6 show the results of a similar series of low-temperature experiments in which other features become more apparent. Spectra were recorded with the samples cooled to  $-196^\circ\text{C}$  to inhibit thermally induced processes and isolate the effects of photon-induced chemical order-

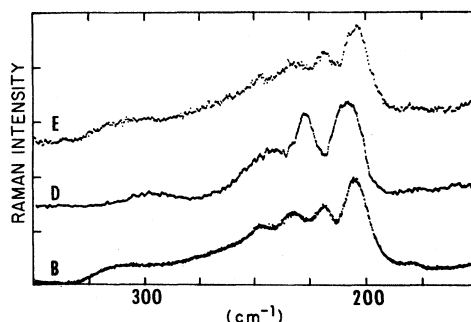


FIG. 5. Expanded view of Fig. 4 from  $150$  to  $350\text{ cm}^{-1}$ .

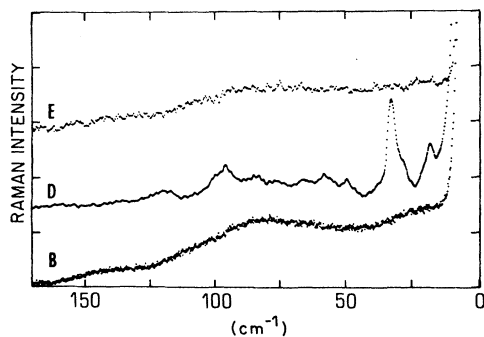


FIG. 6. Expanded view of Fig. 4 from 0 to 170  $\text{cm}^{-1}$ .

ing more unambiguously. With increasing excitation power (Fig. 4 A–4C) no obvious spectral changes occur but in Fig. 4 D several changes are apparent all of which are reminiscent of the photoinduced low-temperature reconstruction of pure  $\text{GeSe}_2$ . The Ge–Ge wrong-bond band disappears. The  $\nu_1$ -like bands for  $(\text{GeSe}_4)$ ,  $(\text{GeSe}_3\text{S})$ , etc. shift to higher frequencies and the low-frequency region becomes rich in narrow Raman lattice bands characteristic of microcrystallites embedded in a glassy matrix. Complete phase separation of microcrystallites from unstressed glass is not indicated, however. The width of the  $\nu_1$  band of the  $(\text{GeSe}_4)$  tetrahedra is too large ( $14 \text{ cm}^{-1}$ ) and a shift of the peak of only  $3.4 \text{ cm}^{-1}$  between Fig. 4 D and B is too small for complete phase separation to have occurred. In pure  $\text{GeSe}_2$  the corresponding shift was the order of  $9 \text{ cm}^{-1}$ . The bandwidth increase and the reduced peak shifts suggest that only poorly defined areas of long-range order exist in this sample as opposed to that of Fig. 3. Annealing the present sample in the dark at room temperature overnight erases the photon-induced changes in the structure (Fig. 4 D, microcrystallinity) and the spectrum reverts to its original state as shown in E of Figs. 4, 5, and 6. The relative proportions of the mixed-chalcogenide linked tetrahedra, however, are not affected by the irradiation or the annealing steps. The equilibrium chemical processes in the melt and the concomitant short-range ordering of nearest neighbors are not affected by below-band-edge photons. The changes that do occur appear to originate at the edges of the structural units (rafts) presumably in the weaker wrong bonds as previously shown for pure  $\text{GeSe}_2$ .<sup>18,26</sup>

Changing the selenium-to-sulfur ratio from 4 to 7 leads to a glass of nominal composition  $\text{GeS}_{0.25}\text{Se}_{1.75}$ , and at this composition  $\text{GeSe}_4$  tetrahedra are almost twice as likely *a priori* as  $\text{GeSSe}_3$  tetrahedra. This sample was heated to  $1025^\circ\text{C}$  instead of  $905^\circ\text{C}$  before quenching to allow a better equilibrium of the chemical processes suggested in Sec. II (short-range order) to occur. Figures 7–9 show the results including the effects of irradiation with increasing laser power. The most obvious difference compared with Figs. 5–7 is the dramatic drop in the relative intensity of the peak at  $217 \text{ cm}^{-1}$  compared to its neighbor at  $202 \text{ cm}^{-1}$ . When this intensity ratio is compared to that observed in Figs. 4 and 5, it is apparent that our assignment of bands in this frequency region to the totally

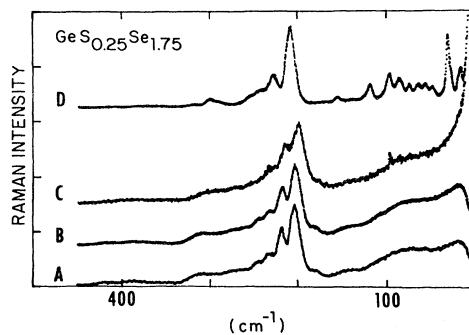


FIG. 7. Raman spectra of  $\text{GeS}_{0.25}\text{Se}_{1.75}$  glass alloy at  $-196^\circ\text{C}$ . Experimental parameters: scan step size,  $0.2 \text{ cm}^{-1}$ ; count time/step in sec, A 1.0, B–D 0.9; spectral slit width,  $4.0 \text{ cm}^{-1}$ . Data smoothing: A, 19-point Savitsky-Golay technique; C, 13-point Savitsky-Golay technique. Laser excitation (in mW) ( $647.1 \text{ nm}$ ): A 4, B 45, C 78, and D 113.

symmetric  $\nu_1$ -type stretching modes in  $(\text{GeSe}_4)$ ,  $(\text{GeSe}_3\text{S})$ ,  $(\text{GeSe}_2\text{S}_2)$ , and  $(\text{GeSeS}_3)$  tetrahedra is basically correct. If the  $217\text{-cm}^{-1}$  band, for example, arose *only* from Se–Se wrong bonds (companion line),<sup>18,26</sup> the present sample, which is more selenium rich compared to that represented by Figs. 4–6, would show a  $217\text{-cm}^{-1}$  band with enhanced intensity over that shown in Figs. 4 and 5.

A second feature of interest appears in C of Figs. 7, 8, and 9. The  $\nu_1$ -related bands have shifted to lower wave numbers and begun to broaden Fig. 8 C, the Ge–Ge wrong-bond band at  $180 \text{ cm}^{-1}$  has begun to weaken (C, Figs. 7 and 8) and at low frequencies the Böse-type band has virtually lost its definition. All of these features indicate significant changes in the glass structure prior to the formation of quasicrystallites and microcrystallites. Similar effects were observed earlier for pure  $\text{GeSe}_2$ .<sup>18,26</sup> Increasing the laser power still further leads to the formation of microcrystallites (D, Figs. 7–9). This is especially evident in D Fig. 9 at low frequencies. The laser power was subsequently increased to the point where the sample cracked into small pieces and therefore it is not known if room-temperature annealing in the dark would have led to reversibility to the glass or not. Data for both samples are summarized in Table III.

As the sulfur content of the  $\text{GeS}_x\text{Se}_{2-x}$  samples are re-

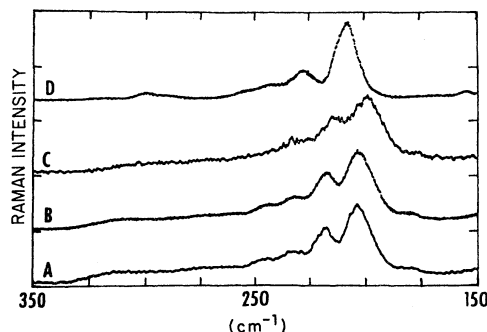


FIG. 8. Expanded view of Fig. 7 from 150 to  $350 \text{ cm}^{-1}$ .

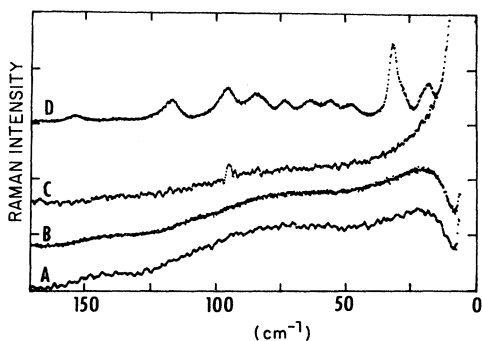


FIG. 9. Expanded view of Fig. 7 from 0 to 170  $\text{cm}^{-1}$ . Asterisk indicates an experimental artifact.

duced to  $x = 0.125$  and  $0.063$ , the intensity distribution of the  $\nu_1$ -like modes should and do change drastically. Those bands due to  $(\text{GeS}_2\text{Se}_2)$  and  $(\text{GeS}_3\text{Se})$  tetrahedra drop relative to the other two,  $(\text{GeSe}_4)$  and  $(\text{GeSSe}_3)$ , as can be seen from the Raman spectrum of  $\text{GeS}_{0.125}\text{Se}_{1.875}$  shown in Fig. 10. The intensity ratio of the  $\nu_1$ -like modes due to  $[(\text{GeSSe}_3)]/[(\text{GeSe}_4)]$  do not change so rapidly which reflects a tradeoff between two important operating factors. As the  $[\text{Se}]/[\text{S}]$  composition ratio increases, the  $[(\text{GeSSe}_3)]/[(\text{GeSe}_4)]$  species-concentration ratio is expected to drop. Simultaneously, however, the band due to Se-Se wrong bonds is expected to increase. Since the energies of these two are nearly accidentally degenerate, the intensity ratio of these contributions— $I_{\nu_1(\text{GeSSe}_3)+\nu(\text{Se-Se})}/I_{\nu_1(\text{GeSe}_4)}$  at  $217 \text{ cm}^{-1}$  for the numerator and  $202 \text{ cm}^{-1}$  for the denominator—does not change

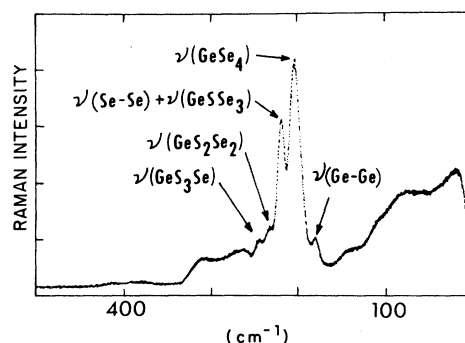


FIG. 10. Raman spectra of  $\text{GeS}_{0.125}\text{Se}_{1.875}$  glass alloy at  $-196^\circ\text{C}$ . Experimental parameters: scan step size,  $0.2 \text{ cm}^{-1}$ ; count time/step, 1.0 sec; spectral slit width,  $3.6 \text{ cm}^{-1}$ ; excitation (647 nm), 100 mW.

nearly so fast as the compositional distribution of tetrahedral species would suggest. The  $\nu_1$ -like bands due to  $(\text{GeS}_2\text{Se}_2)$  and  $(\text{GeS}_3\text{Se})$  tetrahedra are not overlapped in this way, and therefore their intensities more closely reflect their concentrations in the glass structure. Figure 10 shows that the intensities of the bands due to these species are very much lower than the bands at  $217$  and  $202 \text{ cm}^{-1}$ .

This type of information is presented graphically in Fig. 11. Plotted are the intensity ratios of the  $\nu_1$ -like modes  $I_{(\text{GeS}_n\text{Se}_{4-n})}/I_{\text{GeSe}_4}$  as a function of  $x$  in the various  $\text{GeS}_x\text{Se}_{2-x}$  glasses. Thus  $n = 1$  represents  $(\text{GeSSe}_3)$ ,  $n = 2$  represents  $(\text{GeS}_2\text{Se}_2)$ , and so on, and the data is normalized to the intensity of the  $202\text{-cm}^{-1}$  band of the  $(\text{GeSe}_4)$  tetrahedra. The  $n = 1$  curve includes contributions from

TABLE III. Raman spectra of (a)  $\text{GeS}_{0.5}\text{Se}_{1.5}$  and (b)  $\text{GeS}_{0.25}\text{Se}_{1.75}$  glasses and microcrystallites (numerical values are in  $\text{cm}^{-1}$ ).

Glass		Microcrystallites		Assignments <sup>a</sup>
(a)	(b)	(a)	(b)	
21	19	18.7	16.8	Böse peak
		29.0	27.1	
		33.2	30.7	
		50.0	47.4	
		58.3	55.4	
		66.2	63.2	
		76.2	73.2	
82	83	84	84	$\nu_2$ (tetrahedral)
		95.7	95.4	
		126.0	117.0	$\nu_4$ (tetrahedral)
		153.4	153.6	
180	180			$\nu_1$ ( $\text{GeSe}_4$ )
203.9	202.5	207.9	207.4	
217.5	217.5	227.3	227.7	
232.4	231.9	242.1	243.2	
247.7	244.4			
312	312	297.7	300.6	
387	387			
421	423			$\nu_3$ (tetrahedral)

<sup>a</sup>Assignments are for the glass data.

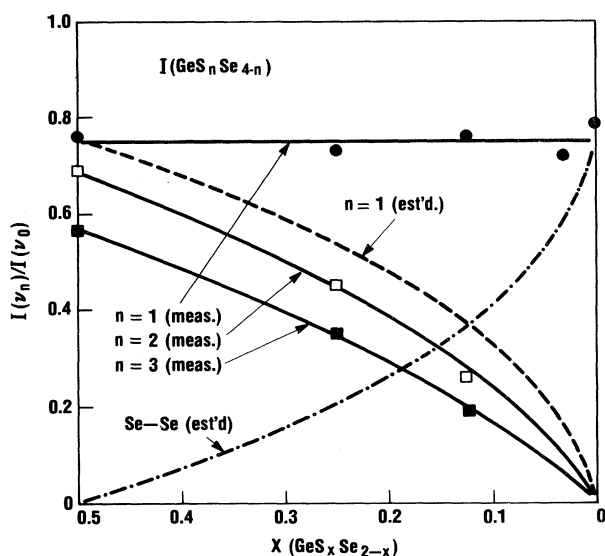


FIG. 11. Intensity ratios of the  $\nu_1$  modes of  $I_{(\text{GeS}_n\text{Se}_{4-n})}/I_{(\text{GeSe}_4)}$  as a function of the sulfur content of  $\text{GeS}_x\text{Se}_{2-x}$  glass alloys. Dashed curve is an estimate of the  $\text{GeSSe}_3$  contribution to the  $n=1$  curve. Dotted-dashed curve is an estimate of the Se—Se wrong-bond contribution to the  $n=1$  curve.

the  $\text{GeSSe}_3$  tetrahedra and the Se—Se wrong bonds. The  $n=2$  and 3 curves contain no contributions from the wrong bond and therefore fall off rapidly as the sulfur content goes toward zero. Based on chemical-equilibria arguments presented earlier, it is expected that the part of the intensity in the  $n=1$  curve of Fig. 11 due to the ( $\text{GeSSe}_3$ ) mode would behave similarly and that the contribution to the band intensity arising from the Se—Se wrong bonds should have a corresponding inverse relationship. The dashed and dotted-dashed curves in Fig. 11 reflect our estimate of those functional relationships. There is a considerable margin for error in these estimates as well as in the measured intensity ratios because of the difficulty in accurately estimating the corrections needed for spectral background contributions and overlapping of individual bands. Such errors can be large. Nevertheless, the major trends shown in Fig. 11 appear to be real and follow expectations.

In support of the estimated curves in Fig. 11 for  $n=1$ , it is worth noting that as  $x$  exceeds 0.5 the glass-forming

tendency decreases precipitously and one obtains compound separation into  $\text{GeSe}_2$  and  $\text{GeS}_2$ . Coincident with this observation, the estimated concentration of Se—Se wrong bonds goes to zero and thus one of the major glass-stabilizing influences built into the models of partially polymerized clusters in  $\text{GeS}_2$  and  $\text{GeSe}_2$  glasses is no longer present.

## VI. SUMMARY

The significant points in the present work include the demonstration (1) of the importance of chemical-equilibrium processes in the melt which determines short-range order in the melt-quenched glass, (2) that photon-induced metamorphoses originate at the edges of structural units (rafts) in the glass, (3) that photon-induced microcrystallization in the  $\text{GeS}_x\text{Se}_{2-x}$  alloys are reversible, (4) that the reversibility is most likely driven by strain at the glass-microcrystallite interface, and (5) that the presence of Se—Se wrong bonds has a strong influence on the glass-forming tendency in mixed-chalcogenide  $\text{GeS}_x\text{Se}_{2-x}$  glasses.

The behavior of these selenium-rich alloys under irradiation with below-band-edge laser light mimics that of pure  $\text{GeSe}_2$ . Thus, although, in the present case, definitive evidence for quasicrystallization enroute to microcrystallization was not presented, it is reasonable to propose that quasicrystallites also occur in the mixed-chalcogenide alloys at the same stage of metamorphosis as in pure  $\text{GeSe}_2$ . Accordingly, we conclude that the ideas presented in more detail earlier for pure- $\text{GeSe}_2$  glass appear to enjoy greater generality than was initially evident. Other work<sup>29</sup> on pure  $\text{GeS}_2$  also supports this contention.

A detailed theoretical analysis of the vibrational splittings reported here for the  $A_1$ -like modes has recently been carried out.<sup>35</sup> One of the interesting conclusions of this work is that at low S concentrations S preferentially replaces Se at corner-sharing sites of the outermost tetrahedral chains. This work also shows that the Se-Se dimer or companion modes actually involve motions of all the Se atoms in the outermost tetrahedra at the edges of the rafts which form corner-sharing chains. This quantitative refinement of our previous analysis<sup>18</sup> in no way changes any of its qualitative conclusions. This is the reason why we continue to refer to these edge-localized modes as Se-Se modes in contradistinction to the Ge-Ge modes of polymerized ethanelike chains.

<sup>1</sup>M. F. Thorpe, in *Vibrational Spectroscopy of Molecular Liquids and Solids*, edited by S. Bratos and R. M. Pick (Plenum, New York, 1979), p. 341.

<sup>2</sup>W. H. Zachariasen, *J. Am. Chem. Soc.* **54**, 3841 (1932).

<sup>3</sup>R. Zallen, in *Fluctuation Phenomena*, edited by E. W. Montroll and J. L. Lebowitz (North-Holland, Amsterdam, 1979), p. 177.

<sup>4</sup>G. S. Cargill, *Ann. N.Y. Acad. Sci.* **279**, 208 (1976).

<sup>5</sup>F. Betts, A. Bienenstock, and S. R. Ovshinsky, *J. Non-Cryst. Solids* **4**, 554 (1970).

<sup>6</sup>R. J. Bell, N. F. Bird, and P. Dean, *Solid State Phys.* **C 1**, 299

(1968).

<sup>7</sup>E. A. Porai-Koshits, *Glastech. Ber.* **32**, 450 (1959).

<sup>8</sup>B. Eckstein, *Mater. Res. Bull.* **3**, 199 (1968); J. E. Stanworth, *Glass Technol.* **17**, 194 (1976).

<sup>9</sup>K. S. Evstropyev and E. A. Porai-Koshits, *J. Non-Cryst. Solids* **11**, 170 (1972).

<sup>10</sup>G. Lucovsky, F. L. Galeener, R. C. Keezer, R. H. Geils, and H. A. Six, *Phys. Rev. B* **10**, 5134 (1974).

<sup>11</sup>G. Lucovsky, F. L. Galeener, R. H. Geils, and R. C. Keezer, in *The Structure of Non-Crystalline Materials*, edited by P. H. Gaskell (Taylor and Francis, London, 1977), p. 127.

- <sup>12</sup>R. J. Nemanich, S. A. Solin, and G. Lucovsky, *Solid State Commun.* **21**, 273 (1977), and references cited therein.
- <sup>13</sup>G. Lucovsky, R. J. Nemanich, and F. L. Galeener, in *Proceedings of the VIIth International Conference on Amorphous and Liquid Semiconductors, Edinburgh, 1977*, edited by W. E. Spear (CICL, University of Edinburgh, Edinburgh, 1977), p. 130, and references cited therein.
- <sup>14</sup>G. Lucovsky, in *Amorphous Semiconductors*, edited by M. Brodsky (Springer, New York, 1979), Vol. 36, p. 215.
- <sup>15</sup>A. Feltz, K. Zichmuller, and G. Pfaff, *Phys. Rev. B* **10**, 125 (1974).
- <sup>16</sup>R. J. Nemanich, G. A. N. Connell, T. M. Hayes, and R. A. Street, *Phys. Rev. B* **18**, 6900 (1978).
- <sup>17</sup>R. A. Street, R. J. Nemanich, and G. A. N. Connell, *Phys. Rev. B* **18**, 6915 (1978).
- <sup>18</sup>P. M. Bridenbaugh, G. P. Espinosa, J. E. Griffiths, J. C. Phillips, and J. P. Remeika, *Phys. Rev. B* **20**, 4140 (1979); N. Kumagai, J. Shirafuji, and Y. Inuishi, *J. Phys. Soc. Jpn.* **42**, 1261 (1977). Further evidence of the unsatisfactory nature of the "rings embedded in a continuous random network" model has been reported for  $g\text{-As}_2\text{S}_3$  by H. Kawamura, K. Fukumasu, and Y. Hamada, *Solid State Commun.* **43**, 229 (1982).
- <sup>19</sup>W. J. Bresser, P. Boolchand, P. Suranyi, and J. P. de Neufville, *Phys. Rev. Lett.* **46**, 1689 (1981).
- <sup>20</sup>P. Boolchand, W. J. Bresser, and M. Tenhover, *Phys. Rev. B* **25**, 2971 (1982).
- <sup>21</sup>P. Boolchand, J. Grothaus, W. J. Bresser, and P. Suranyi, *Phys. Rev. B* **25**, 2975 (1982).
- <sup>22</sup>P. Boolchand, J. Grothaus, and J. C. Phillips, *Solid State Commun.* **45**, 183 (1983).
- <sup>23</sup>J. C. Phillips, *Comments Solid State Phys.* **10**, 165 (1982).
- <sup>24</sup>J. Hajt6, G. Zentai, and I. K6sa-Somogyi, *Solid State Commun.* **23**, 401 (1977).
- <sup>25</sup>J. Hajt6 and P. Apai, *J. Non-Cryst. Solids* **35-6**, 1085 (1980).
- <sup>26</sup>J. E. Griffiths, G. P. Espinosa, J. P. Remeika, and J. C. Phillips, *Solid State Commun.* **40**, 1077 (1981); *Phys. Rev. B* **25**, 1272 (1982).
- <sup>27</sup>J. Hajt6, I. J6nosy, and G. Forg6cs, *J. Phys. C* **15**, 6293 (1982); V. G. Zhdanov, B. T. Kolomiets, V. M. Lyubin, and V. K. Malinovsky, *Phys. Status Solidi* **52**, 621 (1979); V. K. Malinovsky and V. G. Zhdanov, *J. Non-Cryst. Solids* **51**, 31 (1982).
- <sup>28</sup>D. E. Aspnes, J. C. Phillips, and K. L. Tai, *Phys. Rev. B* **23**, 816 (1981); J. C. Phillips, C. A. Beevers, and S. E. B. Gould, *Phys. Rev. B* **21**, 5724 (1980).
- <sup>29</sup>J. E. Griffiths, G. P. Espinosa, J. P. Remeika, and J. C. Phillips (unpublished).
- <sup>30</sup>B. A. Smith, N. Cowlan, and A. M. Shamah, *Philos. Mag. B* **39**, 111 (1979) grew by vapor-transport mixed crystals  $\text{As}_2(\text{Se}_{1-x}\text{S}_x)_3$  for  $0 < x < 0.5$  whose size rapidly decreased with increasing  $x$ . Partial segregation of S-As-S and Se-As-Se chains was inferred from diffraction studies. From these studies it appears that transport kinetics play an important role in S-Se segregation in this system and this suggests that the degree of such segregation in a highly viscous melt may be small. These studies of the good glass former  $\text{As}_2(\text{S,Se})_3$  are analogous to the present investigation. Less analogous but still of interest is the work on  $\text{Sn}(\text{Se}_{1-x}\text{S}_x)_2$  pseudobinary crystals [D. Walsh, S. Jandl, and J. Y. Harbec, *J. Phys.* **13**, L125 (1980)]. Here no alloying-related limitation on crystal size was reported, but localized and nonlocalized modes were identified for  $x > 0.25$ .
- <sup>31</sup>M. L. Delwaulle, F. Francois, and M. Delhay-Buisset, *J. Phys. (Paris)* **15**, 206 (1954).
- <sup>32</sup>M. L. Delwaulle and F. Francois, *C. R. Acad. Sci.* **227**, 1229 (1948).
- <sup>33</sup>C. Cerf and M. B. Delhay, *Bull. Soc. Chim. Fr.* 2818 (1964).
- <sup>34</sup>D. J. Sarrach and J. P. De Neufville, *J. Non-Cryst. Solids* **22**, 245 (1976); A. Hruby, *Czech. J. Phys. B* **23**, 1263 (1973); G. Dittmar and H. Schafer, *Acta Crystallogr. Sect. B* **12**, 1188; **12**, 2726 (1976).
- <sup>35</sup>J. A. Aronovitz, J. R. Banavar, M. A. Marcus, and J. C. Phillips, following paper, *Phys. Rev. B* **28**, 4444 (1983).